Dynamics of influence processes on networks:
Complete mean-field theory; the roles of response functions, connectivity, and synchrony; and applications to social contagion

Kameron Decker Harris,[1, *] Christopher M. Danforth,[1, †] and Peter Sheridan Dodds[1, ‡]

[1]*Department of Mathematics and Statistics, Vermont Advanced Computing Core,*
Vermont Complex Systems Center, and Computational Story Lab,
University of Vermont, Burlington, VT 05405 USA
(Dated: March 7, 2013)

We study binary state dynamics on a network where each node acts in response to the average state of its neighborhood. Allowing varying amounts of stochasticity in both the network and node responses, we find different outcomes in random and deterministic versions of the model. In the limit of a large, dense network, however, we show that these dynamics coincide. We construct a general mean field theory for random networks and show this predicts that the dynamics on the network are a smoothed version of the average response function dynamics. Thus, the behavior of the system can range from steady state to chaotic depending on the response functions, network connectivity, and update synchronicity. As a specific example, we model the competing tendencies of imitation and non-conformity by incorporating an off-threshold into standard threshold models of social contagion. In this way we attempt to capture important aspects of fashions and societal trends. We compare our theory to extensive simulations of this "limited imitation contagion" model on Poisson random graphs, finding agreement between the mean-field theory and stochastic simulations.

I. INTRODUCTION

Networks are an exploding area of research due to the recognition of their generality and ubiquity in physical, biological, technological, and social settings. Dynamical processes taking place on networks are now recognized as the most natural description for a number of phenomena. These include neuron behavior in the brain [1], cellular genetic regulation [2], ecosystem dynamics and stability [3], and infectious diseases [4]. This last category, the study of biological contagion, is in many ways similar to *social* contagion, which refers to the spreading of ideas, fashions, or behaviors among people [5, 6]. This concept underlies the vastly important contemporary area of viral marketing, driven by the ease with which media can be shared and spread through social network websites.

In this work, we present results for a very general model of networked map dynamics, motivated by models of social contagion. Each node has a "response function," a map which determines the state the node will take in response to the states of nodes in its neighborhood. Our model is a type of boolean network [7], and it is closely related to models of percolation [8] and magnetism [7, 9]. We focus on the derivation and analysis of dynamical master equations, both exact and mean-field approximations, that describe the expected evolution of the system state. We also show how certain dense network limits

lead to the convergence of the dynamics to the average response function map dynamics.

We then apply our general theory to a particular limited imitation contagion model [10]. Nodes, representing people, act according to competing tendencies of imitation and non-conformity. One can argue that these two ingredients are essential to all trends; indeed, Simmel, in his classic essay "Fashion" [1957], believed that these are the main forces behind the creation and destruction of fashions. Our model is not meant to be quantitative, except perhaps in carefully designed experiments, but it captures the features with which we are familiar: some trends take off and some do not, and some trends are stable while others vary wildly through time. Our model is closely related to the seminal work of Schelling [12] and Granovetter [13].

In Section II, we define the general model and its deterministic and stochastic variants. In Section III, we provide an analysis of the model when the underlying network is fixed. In Section IV, we develop a mean-field theory of the model on generalized random networks. In Section V, we consider the model on Poisson random networks with a specific kind of response function that reflects the limited imitation we expect in many social contagion processes. For this specific case, we compare the results of simulations and theory. Finally, in Section VI, we present conclusions and directions for further research.

II. GENERAL MODEL

Let $\mathcal{G} = (V, E)$ be a network with $N = |V|$ nodes, where V is the node set and E is the edge set. We let

* Current address: Department of Applied Mathematics, University of Washington, Seattle, WA 98103 USA ; kamdh@uw.edu
† chris.danforth@uvm.edu
‡ peter.dodds@uvm.edu

$A = A(\mathscr{G})$ denote the *adjacency matrix*; entry A_{ij} is the number of edges from node j to node i. Assign each node $i \in V$ a response function $f_i : [0, 1] \to \{0, 1\}$, and let $\mathbf{x}(0) \in \{0, 1\}^N$ be the vector of initial node states. At time step t, each node i computes the fraction

$$\phi_i(t) = \frac{\sum_{j=1}^{N} A_{ij} x_j(t)}{\sum_{j=1}^{N} A_{ij}} \qquad (1)$$

of their neighbors in $\mathscr{G}$ who are active and takes the state

$$x_i(t+1) = f_i(\phi_i(t)) \qquad (2)$$

at the next time step.

The above defines a deterministic dynamical system given a network and set of response functions. This is called a realization of the model [7]. Each node is in either the 0 or 1 state; we refer to these as the off/inactive and on/active states, respectively. In the context of contagion, these would be the susceptible and infected states. With these binary states, our model is a particular kind of Boolean network [7]. Note that each node reacts only to the fraction of its neighbors who are active, rather than the absolute number, and the identities of the input nodes do not matter. Each node's input varies from 0 to 1 in steps of $1/k_i$, where $k_i = \sum_{j=1}^{N} A_{ij}$ is node i's degree (in-degree if $\mathscr{G}$ is not a simple graph).

In the rest of this Section, we will describe some variations of the basic model which also differentiate our model from the Boolean networks extant in the literature. This is mainly due to the response functions, but also the type of random network on which the dynamics take place, varying amounts of stochasticity introduced into the networks and response functions, and the possibility of asynchronous updates.

A. The networks considered

The mean-field analysis in Section IV is applicable to any network which can be characterized by its degree distribution. The vast majority of the theory of random Boolean networks considers only regular random networks. Fortunately, such theories are easily generalized to other types of networks with independently chosen edges, such as Poisson (Erdös-Rényi) and configuration model random networks [9, 14]. We develop specific results for Poisson random networks, and these are the networks considered in Section V.

B. Stochastic variants

The specific network and response functions determine exactly which behaviors are possible. These are chosen from some distribution of networks, such as $\mathcal{G}(N, k_{\text{avg}}/N)$ (Poisson random networks on N nodes with edge probability k_{avg}/N), and some distribution of response functions. In the example of Section V, the response functions

	Rewiring network	Fixed network
Probabilistic response	P-R	P-F
Deterministic response	D-R	D-F

TABLE I. The four different ways we implement the model, corresponding to differing amounts of quenched randomness. These are the combinations of fixed or rewired networks and probabilistic or deterministic response functions. In the thermodynamic limit of the rewired versions, where the network and response functions change every time step, the mean-field theory (Sec. IV) is exact.

are parameterized solely by two thresholds, ϕ_{on} and ϕ_{off}, so the distribution of response functions is determined by the joint density $P(\phi_{\text{on}}, \phi_{\text{off}})$. Again, the specific network and response functions define a realization of the model. When these are fixed for all time, we have, in principle, full knowledge of the possible model dynamics. Given an initial condition $\mathbf{x}(0)$, the dynamics $\mathbf{x}(t)$ are deterministic and known for all $t \geq 0$. As for all finite Boolean networks [7], the system dynamics are eventually periodic, since the state space $\{0, 1\}^N$ is finite.

With the introduction of noise, the system is no longer eventually periodic. Fluctuations at the node level allow a greater exploration of state space, and the behavior is comparable to that of the general class of discrete-time maps. Roughly speaking, the mean-field theory we develop in Section IV becomes more accurate as we introduce more stochasticity.

We introduce randomness in two parts of the model: the network and response functions. Allowing for the network and responses to be either fixed for all time or resampled each time step and taking all possible combinations yields four different designs (see Table I).

1. Rewired networks

First, the network itself can change every time step. This is the rewiring (R), as opposed to fixed (F), network case. For example, we could draw a new network from $\mathcal{G}(N, k_{\text{avg}}/N)$ every time step. This amounts to rewiring the links while keeping the degree distribution fixed, and it is alternately known as a mean field, annealed, or random mixing variant as opposed to a fixed network or quenched model [7].

2. Probabilistic responses

Second, the response functions can change every time step. This is the probabilistic (P), as opposed to the deterministic (D), response function case. For our social contagion example, there needs to be a well-defined distribution $P(\phi_{\text{on}}, \phi_{\text{off}})$ for the thresholds. This amounts to having a single response function, the expected response

function

$$\bar{f}(\phi) = \int d\phi_{\text{on}} \int d\phi_{\text{off}} \, P(\phi_{\text{on}}, \phi_{\text{off}}) f(\phi; \phi_{\text{on}}, \phi_{\text{off}}). \quad (3)$$

We call $\bar{f} : [0,1] \rightarrow [0,1]$ the *probabilistic response function*. Its interpretation is the following. For an updating node with a fraction ϕ of active neighbors at the current time step, then, at the next time step, the node assumes the active state with probability $\bar{f}(\phi)$ and the inactive state with probability $1 - \bar{f}(\phi)$.

3. Temperature in the system

In this paper, the network and response functions are either fixed for all time or resampled every time step. One could tune smoothly between the two extremes by introducing rates at which these reconfigurations occur. These rates are inversely related to quantities that behave like temperature (one for the network and another for the response functions). Holding the network or response functions fixed corresponds to zero temperature, since there are no fluctuations. The stochastic and rewired cases correspond to high or infinite temperature, because reconfigurations occur every time step.

C. Update synchronicity

Finally, we introduce a parameter α for the probability that a given node updates. When $\alpha = 1$, all nodes update each time step, and the update rule is said to be synchronous. When $\alpha \approx 1/N$, only one node is expected to update with each time step, and the update rule is said to be effectively asynchronous. This is equivalent to a randomly ordered sequential update. For intermediate values, α is the expected fraction of nodes which update each time step.

III. FIXED NETWORKS

Consider the case where the response functions and network are fixed (D-F), but the update may be synchronous or asynchronous. Extend the definition of $x_i(t)$ to now be the *probability* that node i is in the active state at time t. Note that this agrees with our previous definition as the *state* of node i when $x_i(t) = 0$ or 1. Then the x_i follow the master equation

$$x_i(t+1) = \alpha f_i \left(\frac{\sum_{j=1}^{N} A_{ij} x_j(t)}{\sum_{j=1}^{N} A_{ij}} \right) + (1-\alpha)x_i(t), \quad (4)$$

which can be written in matrix-vector notation as

$$\mathbf{x}(t+1) = \alpha \, \mathbf{f}(T\mathbf{x}(t)) + (1-\alpha)\mathbf{x}(t). \quad (5)$$

Here $T = D^{-1}A$ is sometimes called the transition probability matrix (since it also occurs in the context of a

random walker), D is the diagonal degree matrix, and $\mathbf{f} = (f_i)$ [15]. If $\alpha = 1$, then $\mathbf{x}(t) \in \{0,1\}^N$ and we recover the fully deterministic response function dynamics given by (1) and (2).

A. Asynchronous limit

Here, we show that when $\alpha \approx 1/N$, time is effectively continuous and the dynamics can be described by an ordinary differential equation. This is similar to the analysis of Gleeson [16]. Consider Eqn. 5. Subtracting $\mathbf{x}(t)$ from both sides and setting $\Delta\mathbf{x}(t) = \mathbf{x}(t+1) - \mathbf{x}(t)$ and $\Delta t = 1$ yields

$$\frac{\Delta\mathbf{x}(t)}{\Delta t} = \alpha \left(\mathbf{f}(T\mathbf{x}(t)) - \mathbf{x}(t) \right). \quad (6)$$

Since α is assumed small, the right hand side is small, and thus $\Delta\mathbf{x}(t)$ is also small. Making the continuum approximation $d\mathbf{x}(t)/dt \approx \Delta\mathbf{x}(t)/\Delta t$ yields the differential equation

$$\frac{d\mathbf{x}}{dt} = \alpha \left(\mathbf{f}(T\mathbf{x}) - \mathbf{x} \right). \quad (7)$$

The parameter α sets the time scale for the system. Below we see that, from their form, similar asynchronous, continuous time limits apply to the dynamical equations in the densely connected case, Eqn. (8), and in the mean-field theory, Eqns. (11) and (12).

B. Dense network limit for Poisson random networks

The following result is particular to Poisson random networks, but similar results are possible for other random networks with dense limits. The normalized Laplacian matrix is defined as $\mathcal{L} \equiv I - D^{-1/2}AD^{-1/2}$, where I is the identity [17]. So $T = D^{-1/2}(I - \mathcal{L})D^{1/2}$. By Oliveira [18], when k_{avg} is $\Omega(\log N)$ there exists a typical Laplacian matrix $\mathcal{L}^{\text{typ}} = I_N - \mathbf{1}_N\mathbf{1}_N^T/N$ such that the actual $\mathcal{L} \approx \mathcal{L}^{\text{typ}}$ in the induced 2-norm with high probability [$\mathbf{1}_N$ is the length-N column vector of ones]. In this limit, if we approximate the degrees as uniform, $k_i \approx k_{\text{avg}}$ for all $i \in V$, then $T \approx T^{\text{typ}} = \mathbf{1}_N\mathbf{1}_N^T/N$. So T effectively averages the node states: $T\mathbf{x}(t) \approx \sum_{i=1}^{N} x_i(t)/N \equiv \phi(t)$. Without a subscript, $\phi(t)$ denotes the active fraction of the network at time t. We make the above approximation in Eqn. 5 and average that equation over all nodes, finding

$$\phi(t+1) = \alpha\bar{f}(\phi(t)) + (1-\alpha)\phi(t) \equiv \Phi(\phi(t); \alpha), \quad (8)$$

where we have assumed that N is large and the average of nodes' individual response functions $\sum_{i=1}^{N} f_i/N$ converges in a suitable sense to the stochastic response function $\bar{f}$, Eqn. (3). This amounts to assuming a law of large numbers for the response functions, i.e., that the

sample average converges to the expected function. Note that α tunes between the probabilistic response function $\Phi(\phi; 1) = \bar{f}(\phi)$ and the line $\Phi(\phi; 0) = \phi$. Also, the fixed points of Φ are fixed points of $\bar{f}$, but their stability will depend on α. When the network is dense, it ceases to affect the dynamics, since each node sees a large number of other nodes. Thus the network is effectively the complete network. In this way we recover the map models of Granovetter and Soong [19].

IV.   MEAN-FIELD THEORY

Making a mean-field calculation refers to replacing the complicated interactions among many particles by a single interaction with some effective external field. There are analogous techniques for understanding network dynamics. Instead of considering the $|E|$ interactions among the N nodes, network mean-field theories derive self-consistent expressions for the overall behavior of the network after averaging over large sets of nodes. These have been fruitful in the study of random Boolean networks [20] and can work well when networks are non-random [21].

We derive a mean-field theory, in the thermodynamic limit, for the dynamics of the general model by blocking nodes according to their degree class. This is equivalent to nodes retaining their degree but rewiring edges every time step. The model is then part of the well-known class of random mixing models with non-uniform contact rates. Probabilistic (P-R) and deterministic (D-R) response functions result in equivalent behavior for these random mixing models. The important state variables end up being the active density of *stubs*, i.e. half-edges or node-edge pairs. In an undirected network without degree-degree correlations, the state is described by a single variable $\rho(t)$. In the presence of correlations we must introduce more variables $\{\rho_k(t)\}$ to deal with the relevant degree classes.

A.   Undirected networks

To derive the mean-field equations in the simplest case—undirected, uncorrelated random networks—consider a degree k node at time t. The probability that the node is in the active state at time $t+1$ given a density ρ of active stubs is

$$F_k(\rho; \bar{f}) = \sum_{j=0}^{k} \binom{k}{j} \rho^j (1-\rho)^{k-j} \bar{f}(j/k), \qquad (9)$$

where each term in the sum counts the contributions from having $0, 1, \ldots, k$ active neighbors. Now, the probability of choosing a random stub which ends at a degree k node is $q_k = kp_k/k_{\text{avg}}$ in an uncorrelated random network [9]. This is sometimes called the edge-degree distribution. So

if all of the nodes update synchronously, the active density of stubs at $t+1$ will be

$$g(\rho; p_k, \bar{f}) = \sum_{k=1}^{\infty} q_k F_k(\rho; \bar{f}) = \sum_{k=1}^{\infty} \frac{kp_k}{k_{\text{avg}}} F_k(\rho; \bar{f}). \quad (10)$$

Finally, if each node only updates with probability α, we have the following map for the density of active stubs:

$$\rho(t+1) = \alpha\, g\left(\rho(t); p_k, \bar{f}\right) + (1-\alpha)\rho(t)$$
$$\equiv G\left(\rho(t); p_k, \bar{f}, \alpha\right). \qquad (11)$$

By a similar argument, the active density of nodes is given by

$$\phi(t+1) = \alpha\, h\left(\rho(t); p_k, \bar{f}\right) + (1-\alpha)\, \phi(t)$$
$$\equiv H\left(\rho(t), \phi(t); p_k, \bar{f}, \alpha\right), \qquad (12)$$

where

$$h(\rho; p_k, f) = \sum_{k=0}^{\infty} p_k F_k(\rho; \bar{f}). \qquad (13)$$

Note that the edge-oriented state variable ρ contains all of the dynamically important information, rather than the node-oriented variable ϕ.

B.   Analysis of the map equation

The function $F_k(\rho; \bar{f})$ is known in polynomial approximation theory as the kth Bernstein polynomial (in the variable ρ) of $\bar{f}$ [22]. Bernstein polynomials have important applications in computer graphics due to their "shape-preserving properties" [23]. The Bernstein operator $\mathbb{B}_k$ takes $\bar{f} \mapsto F_k$. This is a linear, positive operator which preserves convexity for all k and exactly interpolates the endpoints $\bar{f}(0)$ p and $\bar{f}(1)$. Immediate consequences include that each F_k is a smooth function and the kth derivatives $F_k^{(k)}(x) \to \bar{f}^{(k)}(x)$ where $\bar{f}^{(k)}(x)$ exists. For $\bar{f}$ concave down, such as the tent or logistic maps, then F_k is concave down for all k and F_k increases to $\bar{f}$ ($F_k \nearrow \bar{f}$) as $k \to \infty$. This convergence is typically slow. Importantly, $F_k \nearrow \bar{f}$ implies that $g(\rho; p_k, \bar{f}) \leq \bar{f}$ for any degree distribution p_k.

In some cases, the dynamics of the undirected mean-field theory given by $\rho(t+1) = G(\rho(t))$, Eqn. (11), are effectively those of the map Φ, from the dense limit Eqn. (8). We see that g, Eqn. (10), can be seen as the expectation of a sequence of random functions F_k under the edge-degree distribution q_k. Indeed, this is how it was derived. From the convergence of the F_k's, we expect that $g(\rho; p_k, \bar{f}) \approx \bar{f}(\rho)$ if the average degree k_{avg} is "large enough" and the edge-degree distribution has a "sharp enough" peak about k_{avg} (we will clarify this soon). Then as $k_{\text{avg}} \to \infty$, the mean-field coincides with the dense network limit we found for Poisson random networks, Eqn. 8. Some thought leads to a sufficient condition for this kind of convergence: the standard deviation

$\sigma(k_{\mathrm{avg}})$ of the degree distribution must be $o(k_{\mathrm{avg}})$. In Appendix A we prove this as Lemma 1.

In general, if the original degree distribution p_k is characterized by having mean k_{avg}, variance σ^2, and skewness γ_1, then the edge-degree distribution q_k will have mean $k_{\mathrm{avg}} + \sigma^2/k_{\mathrm{avg}}$ and variance $\sigma^2[1 + \gamma_1 \sigma/k_{\mathrm{avg}} - (\sigma/k_{\mathrm{avg}})^2]$. Considering the behavior as $k_{\mathrm{avg}} \to \infty$, we can conclude that requiring $\sigma = o(k_{\mathrm{avg}})$ and $\gamma_1 = o(1)$ are sufficient conditions on p_k to apply Lemma 1. Poisson degree distributions ($\sigma = \sqrt{k_{\mathrm{avg}}}$ and $\gamma_1 = k_{\mathrm{avg}}^{-1/2}$) fit these criteria.

C. Generalized random networks

In more general random networks, nodes can have both undirected and directed incident edges. We denote node degree by a vector $\mathbf{k} = (k^{(\mathrm{u})}, k^{(\mathrm{i})}, k^{(\mathrm{o})})^T$ (for undirected, in-, and out-degree) and write the degree distribution as $p_{\mathbf{k}} \equiv P(\mathbf{k})$. There may also be correlations between node degrees. We encode correlations of this type by the conditional probabilities

$$p_{\mathbf{k},\mathbf{k}'}^{(\mathrm{u})} \equiv P(\mathbf{k}, \mathrm{undirected}|\mathbf{k}')$$
$$p_{\mathbf{k},\mathbf{k}'}^{(\mathrm{i})} \equiv P(\mathbf{k}, \mathrm{incoming}|\mathbf{k}')$$
$$p_{\mathbf{k},\mathbf{k}'}^{(\mathrm{o})} \equiv P(\mathbf{k}, \mathrm{outgoing}|\mathbf{k}'),$$

the probability that an edge starting at a degree $\mathbf{k}'$ node ends at a degree $\mathbf{k}$ node and is, respectively, undirected, incoming, or outgoing relative to the destination degree $\mathbf{k}$ node. We introduced this convention in a series of papers [24, 25]. These conditional probabilities can also be defined in terms of the joint distributions of node types connected by undirected and directed edges. We omit a detailed derivation, since it is similar to that in Section IV A and similar to the equations for the time evolution of a contagion process [24, Eqns. (13–15)] [see also 26].

The result is a coupled system of equations for the density of active stubs which now may depend on node type ($\mathbf{k}$) and edge type (undirected or directed):

$$
\begin{aligned}
\rho_{\mathbf{k}}^{(\mathrm{u})}(t+1) = {} & (1-\alpha)\rho_{\mathbf{k}}^{(\mathrm{u})}(t) + \alpha \sum_{\mathbf{k}'} p_{\mathbf{k},\mathbf{k}'}^{(\mathrm{u})} \sum_{j_u=0}^{k^{(\mathrm{u})'}} \sum_{j_i=0}^{k^{(\mathrm{i})'}} \binom{k^{(\mathrm{u})'}}{j_u} \binom{k^{(\mathrm{i})'}}{j_i} \\
& \times \left[\rho_{\mathbf{k}'}^{(\mathrm{u})}(t)\right]^{j_u} \left[1 - \rho_{\mathbf{k}'}^{(\mathrm{u})}(t)\right]^{(k^{(\mathrm{u})'}-j_u)} \left[\rho_{\mathbf{k}'}^{(\mathrm{i})}(t)\right]^{j_i} \left[1 - \rho_{\mathbf{k}'}^{(\mathrm{i})}(t)\right]^{(k^{(\mathrm{i})'}-j_i)} \\
& \times \bar{f}\left(\frac{j_u + j_i}{k^{(\mathrm{u})'} + k^{(\mathrm{i})'}}\right),
\end{aligned}
\tag{14}
$$

$$
\begin{aligned}
\rho_{\mathbf{k}}^{(\mathrm{i})}(t+1) = {} & (1-\alpha)\rho_{\mathbf{k}}^{(\mathrm{i})}(t) + \alpha \sum_{\mathbf{k}'} p_{\mathbf{k},\mathbf{k}'}^{(\mathrm{i})} \sum_{j_u=0}^{k^{(\mathrm{u})'}} \sum_{j_i=0}^{k^{(\mathrm{i})'}} \binom{k^{(\mathrm{u})'}}{j_u} \binom{k^{(\mathrm{i})'}}{j_i} \\
& \times \left[\rho_{\mathbf{k}'}^{(\mathrm{u})}(t)\right]^{j_u} \left[1 - \rho_{\mathbf{k}'}^{(\mathrm{u})}(t)\right]^{(k^{(\mathrm{u})'}-j_u)} \left[\rho_{\mathbf{k}'}^{(\mathrm{i})}(t)\right]^{j_i} \left[1 - \rho_{\mathbf{k}'}^{(\mathrm{i})}(t)\right]^{(k^{(\mathrm{i})'}-j_i)} \\
& \times \bar{f}\left(\frac{j_u + j_i}{k^{(\mathrm{u})'} + k^{(\mathrm{i})'}}\right).
\end{aligned}
\tag{15}
$$

The active fraction of nodes at a given time is

$$
\begin{aligned}
\phi(t+1) = {} & (1-\alpha)\phi(t) + \alpha \sum_{\mathbf{k}} p_{\mathbf{k}} \sum_{j_u=0}^{k^{(\mathrm{u})}} \sum_{j_i=0}^{k^{(\mathrm{i})}} \binom{k^{(\mathrm{u})}}{j_u} \binom{k^{(\mathrm{i})}}{j_i} \\
& \times \left[\rho_{\mathbf{k}}^{(\mathrm{u})}(t)\right]^{j_u} \left[1 - \rho_{\mathbf{k}}^{(\mathrm{u})}(t)\right]^{(k^{(\mathrm{u})}-j_u)} \left[\rho_{\mathbf{k}}^{(\mathrm{i})}(t)\right]^{j_i} \left[1 - \rho_{\mathbf{k}}^{(\mathrm{i})}(t)\right]^{(k^{(\mathrm{i})}-j_i)} \\
& \times \bar{f}\left(\frac{j_u + j_i}{k^{(\mathrm{u})} + k^{(\mathrm{i})}}\right).
\end{aligned}
\tag{16}
$$

Because these expressions are very similar to the undirected case, we expect similar convergence properties to those in Sec. IV B. However, an explicit investigation of this convergence is beyond the scope of the current paper.

V. LIMITED IMITATION CONTAGION MODEL

As a motivating example of these networked map dynamics, we study an extension of the classical threshold

models of social contagion [such as 12, 13, 27–29, among others]. What differentiates our limited imitation contagion model from the standard models is that the response function includes an off-threshold, above which the node takes the inactive state. We assign each node $i \in V$ an on-threshold $\phi_{\mathrm{on},i}$ and an off-threshold $\phi_{\mathrm{off},i}$, requiring $0 \leq \phi_{\mathrm{on},i} \leq \phi_{\mathrm{off},i} \leq 1$. Node i's response function $f_i(\phi_i) = f_i(\phi_i; \phi_{\mathrm{on},i}, \phi_{\mathrm{off},i})$ is 1 if $\phi_{\mathrm{on},i} \leq \phi_i \leq \phi_{\mathrm{off},i}$ and 0 otherwise. See Figure 1 for an example on-off threshold response function.

This is exactly the model of Granovetter and Soong [19], but on a network. We motivate this choice with the following [also see 19]. (1) Imitation: the on state becomes favored as the fraction of active neighbors surpasses the on-threshold (bandwagon effect). (2) Nonconformity: the on state is eventually less favorable with the fraction of active neighbors past the off-threshold (reverse bandwagon, snob effect). (3) Simplicity: in the absence of any raw data of "actual" response functions, which are surely highly context-dependent and variable, we choose arguably the simplest deterministic functions which capture imitation and non-conformity.

A crucial difference between our model and many related threshold models is that, in those models, an activated node can never reenter the susceptible state. Gleeson and Cahalane [26] call this the permanently active property and elaborate on its importance to their analysis. Such models must eventually reach a steady state. When the dynamics are deterministic, this will be some fixed fraction of active nodes. The introduction of the off-threshold builds in a mechanism for node deactivation. Because nodes can now recurrently transition between on and off states, the deterministic dynamics can exhibit a chaotic transient (as in random boolean networks [7]), and the long time behavior can be periodic with potentially high period. With stochasticity, the dynamics can be truly chaotic.

The networks we consider are Poisson random networks from $\mathcal{G}(N, k_{\mathrm{avg}}/N)$. The thresholds ϕ_{on} and ϕ_{off} are distributed uniformly on $[0, 1/2)$ and $[1/2, 1]$, respectively. This distribution results in the probabilistic response function (see Figure 2)

$$\bar{f}(\phi) = \begin{cases} 2\phi & \text{if } 0 \leq \phi < 1/2, \\ 2 - 2\phi & \text{if } 1/2 \leq \phi \leq 1. \end{cases} \qquad (17)$$

The tent map is a well-known chaotic map of the unit interval [30]. We thus expect the limited imitation model with this probabilistic response function to exhibit similarly interesting behavior.
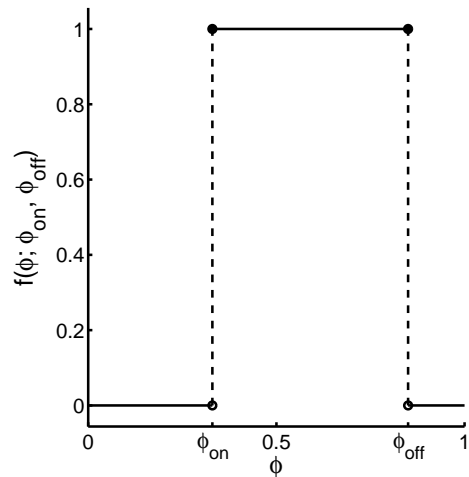

FIG. 1. An example on-off threshold response function. Here, $\phi_{\mathrm{on}} = 0.33$ and $\phi_{\mathrm{off}} = 0.85$. The node will "activate" if $\phi_{\mathrm{on}} \leq \phi \leq \phi_{\mathrm{off}}$, where ϕ is the fraction of its neighbors who are active. Otherwise it takes the "inactive" state.
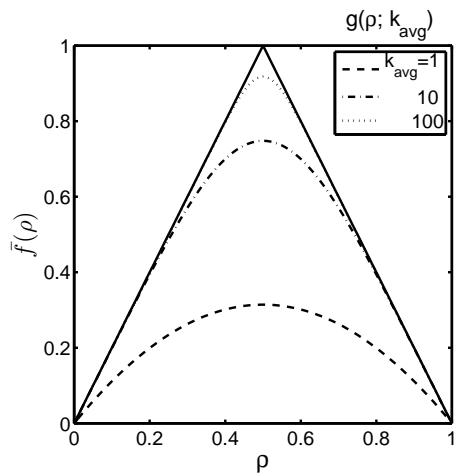

FIG. 2. The tent map probabilistic response function $\bar{f}(\rho)$, Eqn. (17), used in the limited imitation contagion model. This is compared to the edge maps $g(\rho; k_{\mathrm{avg}}) = g(\rho; p_k, \bar{f})$, Eqn. (10), shown for $k_{\mathrm{avg}} = 1, 10, 100$. These p_k are Poisson distributions with mean k_{avg}. As k_{avg} increases, $g(\rho; k_{\mathrm{avg}})$ increases to $\bar{f}(\rho)$.

A. Analysis of the dense limit

When the network is in the dense limit (Section III B), the dynamics follow $\phi(t+1) = \Phi(\phi(t); \alpha)$, where

$$\Phi(\phi; \alpha) = \alpha \bar{f}(\phi) + (1 - \alpha)\phi$$
$$= \begin{cases} (1+\alpha)\phi & \text{if } 0 \leq \phi < 1/2, \\ (1-3\alpha)\phi + 2\alpha & \text{if } 1/2 \leq \phi \leq 1. \end{cases} \qquad (18)$$

Solving for the fixed points of $\Phi(\phi; \alpha)$, we find one at $\phi = 0$ and another at $\phi = 2/3$. When $\alpha < 2/3$, the nonzero fixed point is attracting for all initial conditions
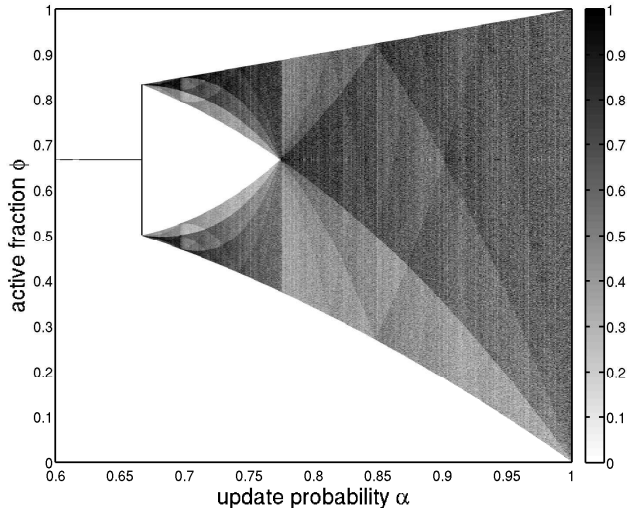
FIG. 3. Bifurcation diagram for the dense map $\Phi(\phi;\alpha)$, Eqn. (18). This was generated by iterating the map at 1000 α values between 0 and 1. The iteration was carried out with 3 random initial conditions for 10000 time steps each, discarding the first 1000. The ϕ-axis contains 1000 bins and the invariant density, shown by the grayscale value, is normalized by the maximum for each α. With $\alpha < 2/3$, all trajectories go to the fixed point at $\phi = 2/3$.

except $\phi = 0$. When $\alpha = 2/3$, $[1/2, 5/6]$ is an interval of period-2 centers. Any orbit will eventually land on one of these period-2 orbits. When $\alpha > 2/3$, this interval of period-2 centers ceases to exist, and more complicated behavior ensues. Figure 3 shows the bifurcation diagram for $\Phi(\phi;\alpha)$. From the bifurcation diagram, the orbit appears to cover dense subsets of the unit interval when $\alpha > 2/3$. The bifurcation diagram appears like that of the tent map (not shown; see [10, 30]) except the branches to the right of the first bifurcation point are separated here by the interval of period-2 centers.

The effect of conformsits, an aside

Suppose some fraction c of the population is made up of individuals without any off-threshold (alternatively, each of their off-thresholds $\phi_{\text{off}} = 1$). These individuals are conformist or "purely pro-social" in the sense that they are perfectly happy being part of the majority. For simplicity, assume $\alpha = 1$. The map $\Phi(\phi; c) = 2\phi$ for $0 \leq \phi < 1/2$ and $2 - 2(1-c)\phi$ for $1/2 \leq \phi \leq 1$. If $c > 1/2$, then the equilibrium at $2/3$ is stable. Pure conformists, then, can have a stabilizing effect on the process. We expect a similar effect when the network is not dense.

B. Mean-field

Here we show how we compute the mean-field maps derived in Section IV. In this specific example, we can write the degree-dependent map $F_k(\rho; \bar{f})$ in terms of incomplete regularized beta functions $I_z(a,b)$ [31]. Since $\bar{f}$ is understood to be the tent map, we will write $F_k(\rho; \bar{f}) = F_k(\rho)$. We find that

$$F_k(\rho) = 2\rho - 4\rho I_\rho(M, k - M), \qquad (19)$$

where we have let $M = \lfloor k/2 \rfloor$ for clarity ($\lfloor \cdot \rfloor$ and $\lceil \cdot \rceil$ are the floor and ceiling functions). The details of this derivation are given in Appendix B.

The map $g(\rho; p_k, \bar{f})$ is parametrized here by the network parameter k_{avg}, since p_k is fixed as a Poisson distribution with mean k_{avg} and $\bar{f}$ is the tent map, and we write it as simply $g(\rho; k_{\text{avg}})$. To evaluate $g(\rho; k_{\text{avg}})$, we compute $F_k(\rho)$ using Eqn. (19) and constrain the sum in Eqn. (10) to values of k with $\lfloor k_{\text{avg}} - 3\sqrt{k_{\text{avg}}} \rfloor \leq k \leq \lceil k_{\text{avg}} + 3\sqrt{k_{\text{avg}}} \rceil$. This computes contributions to within three standard deviations of the average degree in the network, requiring only $O(\sqrt{k_{\text{avg}}})$ evaluations of Eqn. (19). The representation in Eqn. (19) allows for quick numerical evaluation of $F_k(\rho)$ for any k, which we performed in MATLAB.

In Figure 2, we show $g(\rho; k_{\text{avg}})$ for $k_{\text{avg}} = 1, 10$, and 100. We confirm the conclusions of Section IV B: $g(\rho; k_{\text{avg}})$ is bounded above by $\bar{f}(\rho)$, and $g(\rho; k_{\text{avg}}) \nearrow \bar{f}(\rho)$ as $k_{\text{avg}} \to \infty$. Convergence is slowest at $\rho = 1/2$, where the kink exhibited by the tent map has been smoothed out by the effect of the Bernstein operator.

C. Simulations

We performed stochastic simulations of the limited imitation model for the D-F, P-F, and P-R designs, in the abbreviations of Table I. Unless otherwise noted, $N = 10^4$. For all of the bifurcation diagrams, the first 3000 time steps were considered transient and discarded, and the invariant density of ρ was calculated from the following 1000 points. For plotting purposes, the invariant density was normalized by its maximum at those parameters. For example, in Figure 3 we plot $P(\phi|\alpha)/\max_\phi P(\phi|\alpha)$ rather than the raw density $P(\phi|\alpha)$.

To compare the mean-field theory to those simulations, we numerically iterated the edge map $\rho(t+1) = G(\rho(t); k_{\text{avg}}, \alpha)$ for different values of α and k_{avg}. We then created bifurcation diagrams of the possible behavior in the mean-field as was done for the simulations.

D. Results

To provide a feel for the deterministic dynamics, we show the result of running the D-F model on a small network in Figure 4. Here, $N = 100$ and $k_{\text{avg}} = 17$. Starting
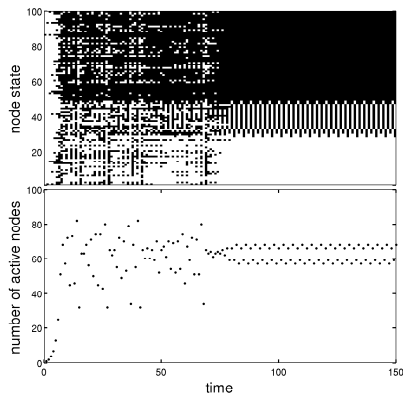
FIG. 4. Deterministic (D-F) dynamics on a small network. Here, $N = 100$ and $k_{\mathrm{avg}} = 17$. On the left, we plot the state evolution over time. The upper plot shows individual node states (black = active) sorted by their eventual level of activity, and the lower plot shows the total number of active nodes. We see that the contagion takes off, followed by a transient period of unstable behavior until time step 80, when the system enters a macroperiod-4 orbit. Note that individual nodes exhibit different microperiods (see Sec. V D). On the right, we show the network itself with the initial seed node in black in the lower right.

from a single initially active node at $t = 0$, the active population grows monotonically over the next 6 time steps. From $t = 6$ to $t = 80$, the transient time, the active fraction varies in a similar manner to the dynamics in the stochastic and mean-field cases. After the transient, the state collapses into a period-4 orbit. We call the overall period of the system its "macroperiod," while individual nodes may exhibit different "microperiods." Note that the macroperiod is the lowest common multiple of the individual nodes' microperiods. In Figure 4, we observe microperiods 1, 2, and 4 in the timeseries of individual node activity. In other networks, we have observed up to macroperiod 240 [10]. A majority of the nodes end up frozen in the on or off state, with approximately 20% of the nodes exhibiting cyclical behavior after collapse. The focus of this paper has been the analysis of the on-off threshold model, and the D-F case has not been as amenable to analysis as the stochastic cases. We offer a deeper examination through simulation of the deterministic case in [10].

We explore the mean-field dynamics by examining the limiting behavior of the active edge fraction ρ under the map $G(\rho; k_{\mathrm{avg}}, \alpha)$. We simulated the map dynamics for a mesh of points in the $(k_{\mathrm{avg}}, \alpha)$ plane. We plot the 3-dimensional (3-d) bifurcation structure of the mean-field theory in Figure 5. We also show 2-d bifurcation plots for fixed k_{avg} and α slices through this volume in Figures 6 and 7. For more visualizations of this bifurcation structure, see Appendix C. In all cases, the invariant density of ρ is normalized by its maximum for that $(k_{\mathrm{avg}}, \alpha)$ pair and indicated by the grayscale value.
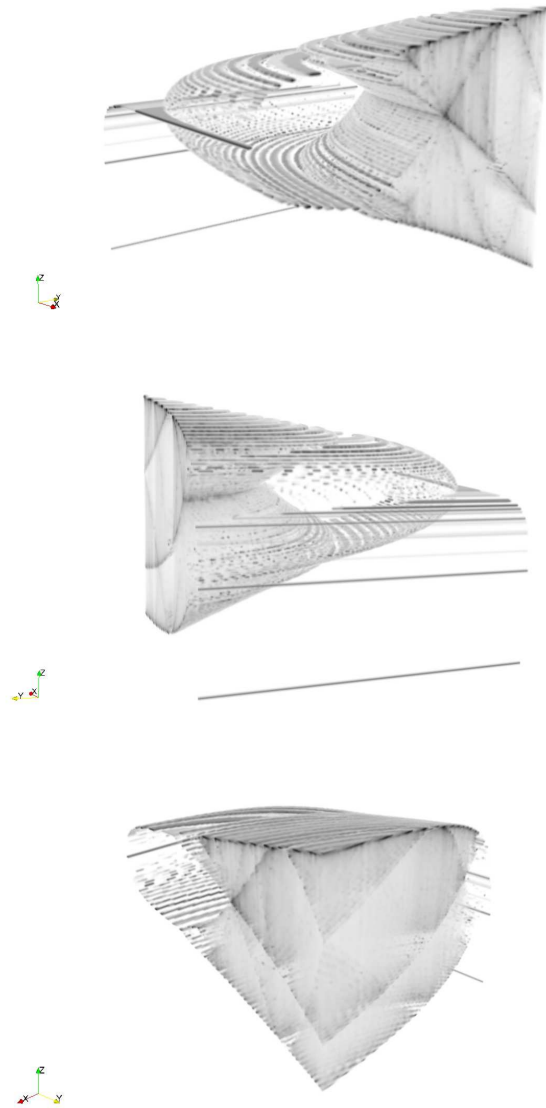

FIG. 5. The 3-dimensional bifurcation diagram computed from the mean-field theory. The axes X = average degree k_{avg}, Y = update probability α, and Z = active edge fraction ρ. The discontinuities of the surface are due to the limited resolution of our simulations. See Figure 6 for the parameters used. This was visualized using Paraview, and a file is available in the online Appendix.

The mean-field map dynamics exhibit period-doubling bifurcations in both parameters k_{avg} and α. Visualizing the bifurcation structure in 3-d (Figure 5) shows interlacing period-doubling cascades in the two parameter dimensions. These bifurcations are more clearly resolved when we take slices of the volume for fixed parameter values. The mean-field theory (Figure 6) closely matches the P-R simulations (Figure 7). The first derivative $\frac{\partial G}{\partial \rho}(\rho; k_{\mathrm{avg}}, \alpha) < \frac{\partial \Phi}{\partial \rho}(\rho; \alpha)$ for any finite k_{avg}, so the bifurcation point $\alpha = 2/3$ which we found for the dense
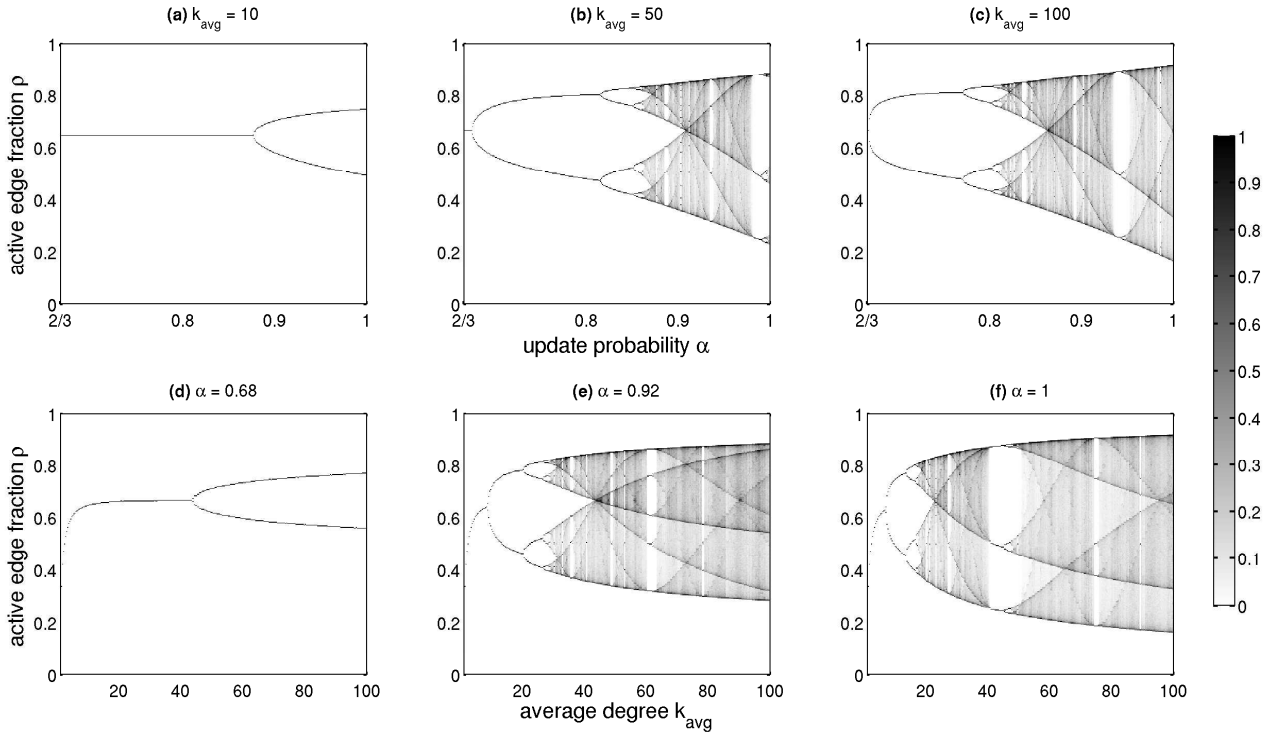
FIG. 6. Mean-field theory bifurcation diagram slices for various fixed values of k_{avg} and α. The top row (a–c) shows slices for fixed k_{avg}. As $k_{\mathrm{avg}} \to \infty$, the k_{avg}-slice bifurcation diagram asymptotically approaches the bifurcation diagram for the dense map, Figure 3. Note that the first bifurcation point, near 2/3, grows steeper with increasing k_{avg}. The bottom row (d–f) shows slices for fixed α. The resolution of the simulations was $\alpha = 0.664, 0.665, \ldots, 1$, $k_{\mathrm{avg}} = 1, 1.33, \ldots, 100$, and ρ bins were made for 1000 points between 0 and 1.
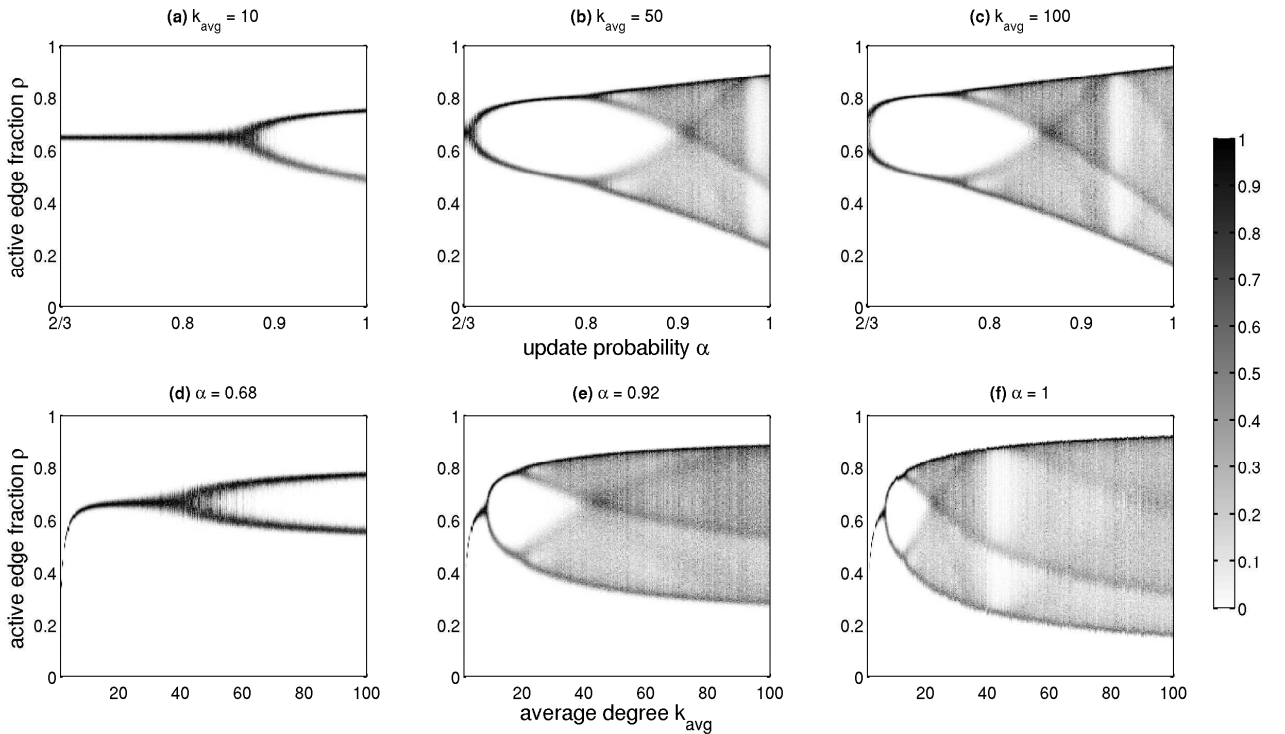

FIG. 7. Bifurcation diagram from fully stochastic (P-R) simulations, made in the same way as Figure 6. The bifurcation structure of these stochastic simulations matches that of the mean-field theory (Figure 6), albeit with some blurring.

map Φ is an upper bound for the first bifurcation point of G. The actual location of the first bifurcation point depends on k_{avg}, but $\alpha = 2/3$ becomes more accurate for higher k_{avg} (it is an excellent approximation in Figures 6c and 7c, where $k_{\mathrm{avg}} = 100$). When $\alpha = 1$, the first bifurcation point occurs at $k_{\mathrm{avg}} \approx 7$.

The bifurcation diagram slices resemble each other and evidently fall into the same universality class as the logistic map [32, 33]. This class contains all 1-d maps with a single, locally-quadratic maximum. Due to the properties of the Bernstein polynomials, $F_k(\rho; \bar{f})$ will universally have such a quadratic maximum for any concave down, continuous $\bar{f}$ [22]. So this will also be true for $g(\rho; k_{\mathrm{avg}}, \bar{f})$ with k_{avg} finite, and we see that k_{avg} partially determines the amplitude of that maximum in Figure 2. Thus k_{avg} acts as a bifurcation parameter. The parameter α tunes between $G(\rho; k_{\mathrm{avg}}, 1) = g(\rho; k_{\mathrm{avg}}, \bar{f})$ and $G(\rho; k_{\mathrm{avg}}, 0) = \rho$, so it has a similar effect. Note that the tent map $\bar{f}$ and the dense limit map Φ are kinked at their maxima, so their bifurcation diagrams are qualitatively different from those of the mean-field. The network, by constraining the interactions among the population, causes the mean-field behavior to fall into a different universality class than the individual response function map.

VI. CONCLUSIONS

We have described a very general class of synchronous or asynchronous, binary state dynamics occuring on networks. We obtained an exact master equation and showed that, when random networks are sufficiently dense, the networked dynamics approach those of the fully-connected case. We developed a mean-field theory and found that it also predicted the same limiting behavior. The convergence of the mean-field map to the average response function is related to the Bernstein polynomials, allowing us to employ many previous results in order to analyze the mean-field map equation. We also extended those mean-field equations to correlated random networks.

The general model we describe was motivated by the the limited imitation model of social contagion. We see that including an aversion to total conformity results in more complicated, even chaotic dynamics, as opposed to the simple spreading behavior typically seen in the single threshold case. The theory developed for the general case successfully captured the behavior of the stochastic network dynamics. We have focused on the rich structure of bifurcations as the two parameters, update synchronicity α and average degree k_{avg}, were varied. We see that the universality class of the dynamics matches those of the logistic map. Using the mean-field theory, we can understand this as a result of the smoothing effect of the Bernstein polynomials on the tent map average response function. However, this universality class will appear for any unimodal, concave down response function.

The deterministic case, which we have barely touched on here, merits further study [see 10]. In particular, we would like to characterize the distribution of periodic sinks, how the collapse time scales with system size, and how similar the transient dynamics are to the mean-field dynamics.

Furthermore, the model should be tested on realistic networks. These could include power law or small world random networks, or real social networks gleaned from data. In a manner similar to Melnik et al. [21], one could evaluate the accuracy of the mean-field theory for real networks.

Finally, the ultimate validation of this model would emerge from a better understanding of social dynamics themselves. Characterization of people's "real" response functions is therefore critical [some work has gone in this direction; see 5, 6, 34, 35]. Comparison of model output to large data sets, such as observational data from social media or online experiments, is an area for further experimentation. This might lead to more complicated context- and history-dependent models. As we collect more data and refine experiments, the eventual goal of quantifiably predicting social behavior, including fashions and trends, seems achievable.

Appendix A: Proof of Lemma 1

Lemma 1. *For $k \geq 1$, let f_k be continuous real-valued functions on a compact domain X with $f_k \to f$ uniformly. Let p_k be a probability mass function on $\mathbb{Z}^+$ parametrized by its mean μ and with standard deviation $\sigma(\mu)$, assumed to be $o(\mu)$. Then,*

$$\lim_{\mu \to \infty} \left(\sum_{k=0}^{\infty} p_k f_k \right) = f.$$

Proof. Suppose $0 \leq a < 1$ and let $K = \lfloor \mu - \mu^a \rfloor$. Then,

$$g = \sum_{k=0}^{\infty} p_k f_k = \sum_{k=0}^{K} p_k f_k + \sum_{k=K+1}^{\infty} p_k f_k. \qquad (A1)$$

Since $f_k \to f$ uniformly as $k \to \infty$, for any $\epsilon > 0$ we can choose μ large enough that

$$|f_k(x) - f(x)| < \epsilon \qquad (A2)$$

for all $k > K$ and all $x \in X$. Without loss of generality, assume that $|f_k| \le 1$ for all k. Then,

$$|g - f| \le \left(\frac{\sigma}{\mu^a}\right)^2 + \epsilon.$$

The σ/μ^a term is a consequence of the Chebyshev inequality [14] applied to the first sum in (A1). Since σ grows sublinearly in μ, this term vanishes for some $0 \le a < 1$ when we take the limit $\mu \to \infty$. The ϵ term comes from using (A2) in the second sum in (A1), and it can be made arbitrarily small. □

Appendix B: Beta function representation of F_k

We now show how, when $\bar{f}$ is the tent map (17), the degree-k map $F_k(\rho; \bar{f})$ can be written in terms of incomplete regularized beta functions. First, use the piecewise

form of Eqn. (17) to write

$$
\begin{aligned}
F_k(\rho) &= \sum_{j=0}^{M} \binom{k}{j} \rho^j (1-\rho)^{k-j} \left(\frac{2j}{k}\right) \\
&\quad + \sum_{j=M+1}^{k} \binom{k}{j} \rho^j (1-\rho)^{k-j} \left(2 - \frac{2j}{k}\right) \\
&= 2 - 2\rho - 2 \sum_{j=0}^{M} \binom{k}{j} \rho^j (1-\rho)^{k-j} \\
&\quad + \left(\frac{4}{k}\right) \sum_{j=0}^{M} \binom{k}{j} \rho^j (1-\rho)^{k-j} j. \quad \text{(B1)}
\end{aligned}
$$

We have used the fact that the binomial distribution $\binom{k}{j} \rho^j (1-\rho)^{k-j}$ sums to one and has mean $k\rho$. For $n \le M$, we have the identity

$$
\sum_{j=0}^{M} (j)_n \binom{k}{j} \rho^j (1-\rho)^{k-j} = \rho^n (k)_n I_{1-\rho}(k-M, M-n+1)
$$
(B2)

where $I_x(a, b)$ is the regularized incomplete beta function and $(k)_n = k(k-1) \cdots (k-(n-1))$ is the falling factorial [31, 36]. This is an expression for the partial (up to M) nth factorial moment of the binomial distribution with parameters k and ρ. Note that when $n = 0$ we recover the well-known expression for the binomial cumulative distribution function. From Eqns. (B1) and (B2), we arrive at Eqn. (19).

Appendix C: Online material

To better explore the 3-d mean field bifurcation structure, we created movies of the the k_{avg} and α slices as the parameters are dialed. We also provide a VTK file with the 3-d bifurcation data, viewable in Paraview or other software. Videos of the individual-node dynamics for small networks in the D-F and P-F cases are shown for some parameters which produce interesting behavior. The D-F, P-F, and P-R cases were implemented in Python, and we provide our code. All of the above is available from http://www.uvm.edu/storylab/share/papers/harris2013a/.

[1] S. Coombes, B. Doiron, K. Josić, and E. Shea-Brown, Philosophical Transactions of the Royal Society A: Mathematical, Physical and Engineering Sciences **364**, 3301 (2006).

[2] R. Milo, S. Shen-Orr, S. Itzkovitz, N. Kashtan, D. Chklovskii, and U. Alon, Science **298**, 824 (2002).

[3] J. Bascompte, Science **325**, 416 (2009).

[4] P. Rohani, X. Zhong, and A. King, Science **330**, 982 (2010).

[5] J. Ugander, L. Backstrom, C. Marlow, and J. Kleinberg, PNAS **109**, 5962 (2012).

[6] D. Centola, Science **329**, 1194 (2010).

[7] M. Aldana, S. Coppersmith, and L. P. Kadanoff, in *Perspectives and Problems in Nonlinear Science*, edited by E. Kaplan, J. E. Marsden, and K. R. Sreeni-

vasan (Springer, New York, 2003), chap. 2, pp. 23–90, http://arxiv.org/abs/nlin/0204062.

[8] D. Stauffer and A. Aharony, *Introduction to Percolation Theory* (Taylor and Francis, London, 1994), 2nd ed.

[9] M. E. J. Newman, SIAM Review **45**, 167 (2003).

[10] P. S. Dodds, K. D. Harris, and C. M. Danforth (2013), http://arxiv.org/abs/1208.0255.

[11] G. Simmel, American Journal of Sociology **62**, 541 (1957).

[12] T. C. Schelling, Journal of Mathematical Sociology **1**, 143 (1971).

[13] M. Granovetter, American Journal of Sociology **83**, 1420 (1978).

[14] B. Bollobás, *Random Graphs* (Cambridge University Press, 2001), 2nd ed.

[15] When there are isolated nodes, those nodes' degrees are 0, and thus the denominator in the master equation is zero and D^{-1} undefined. If the initial network contains isolated nodes, we set all entries in the corresponding rows of T to zero.

[16] J. P. Gleeson, Phys. Rev. E **77**, 046117 (2008).

[17] D. B. West, *Introduction to Graph Theory* (Prentice Hall, Upper Saddle River, NJ, 2001), 2nd ed.

[18] R. I. Oliveira (2010), http://arxiv.org/abs/0911.0600, 0911.0600.

[19] M. Granovetter and R. Soong, Journal of Economic Behavior and Organization **7**, 83 (1986).

[20] B. Derrida and Y. Pomeau, Europhys. Lett. **1**, 45 (1986).

[21] S. Melnik, A. Hackett, M. A. Porter, P. J. Mucha, and J. P. Gleeson, Phys. Rev. E **83**, 036112 (2011).

[22] G. M. Phillips, *Interpolation and Approximation by Polynomials* (Springer, 2003), see chapter 7.

[23] J. M. Peña, ed., *Shape Preserving Representations in Computer-Aided Geometric Design* (Nova Science Publishers, Inc, 1999).

[24] J. L. Payne, K. D. Harris, and P. S. Dodds, Phys. Rev. E **84**, 016110 (2011), URL http://link.aps.org/doi/10.1103/PhysRevE.84.016110.

[25] P. S. Dodds, K. D. Harris, and J. L. Payne, Phys. Rev. E **83**, 056122 (2011), URL http://link.aps.org/doi/10.1103/PhysRevE.83.056122.

[26] J. P. Gleeson and D. J. Cahalane, Phys. Rev. E **75**, 056103 (2007), URL http://link.aps.org/doi/10.1103/PhysRevE.75.056103.

[27] T. C. Schelling, Journal of Conflict Resolution **17**, 381 (1973).

[28] D. J. Watts, PNAS **99**, 5766 (2002).

[29] P. S. Dodds and D. J. Watts, Phys. Rev. Lett. **92**, 218701 (2004).

[30] K. T. Alligood, T. D. Sauer, and J. A. Yorke, *Chaos: An Introduction to Dynamical Systems* (Springer, 1996).

[31] NIST, *Digital Library of Mathematical Functions* (2012), http://dlmf.nist.gov.

[32] M. J. Feigenbaum, Journal of Statistical Physics **19**, 25 (1978).

[33] M. J. Feigenbaum, Journal of Statistical Physics **21**, 669 (1979).

[34] D. Centola, Science **334**, 1269 (2011).

[35] D. M. Romero, B. Meeder, and J. Kleinberg, in *Proc. 20th ACM International World Wide Web Conference* (2011).

[36] R. L. Winkler, G. M. Roodman, and R. R. Britney, Management Science **19**, 290 (1972).